Woody plants optimize stomatal behavior relative to hydraulic risk

Supporting Information

Supplementary Methods

Dataset processing

In four of the tropical understory plants, measurements from extremely low light conditions (PAR < 70 μmol m^{-2} s^{-1}) were excluded because the plant was estimated to be in negative carbon balance unrelated to water stress. Excluding these is unlikely to change the cost function calculations, as they would be entirely during low water stress conditions and the cost functions should mostly diverge during dry conditions (Fig 1). Leaf temperatures were not available for 1 species (*Prosopis velutina*) and thus leaf temperatures were assumed to be air temperature for that species.

MXTE functional form

Because the MXTE is the derivative of the cost function, this linear formulation of the MXTE assumes a parabolic functional form of the costs/risk of low water potential (e.g. Equation 9). This was chosen because it had the fewest parameters that allowed distinguishing whether observed MXTE was constant/increasing (CM) or decreasing (WUE) with more negative ψ_L (Fig. 1a) and can capture a general threshold pattern in response to changing ψ_L with a relatively constant region around the parabola maximum/minimum and then a quadratically increasing or decreasing risk as water potentials decline.

Sensitivity analyses and statistics

The bootstrap analysis using the input driving data should capture much of the potential error within driving variables and measurements within the estimated 95% confidence intervals for the cost function parameters (e.g. Fig 3). We next examined the sensitivity of the stomatal cost function to species' traits in a sensitivity analysis. The estimated K_{max} and V_{cmax} were varied independently +/- 10% for a representative subset of species (Table S4). The parameter estimation procedure was run as described above with the new parameter values.

Controls of the MXTE slope were tested against the hydraulic traits (c and d parameters of the xylem vulnerability curve), mean annual precipitation and temperature of the species drawn from the source studies, V_{cmax}, and percent loss of stomatal conductance (g_s) during the most water-stressed measurement divided by the percent loss of hydraulic conductivity of stems (K) during the most water-stressed measurement. We used ordinary least-squares linear models with weighting based on the inverse of the variance based on bootstrapping. We verified the appropriateness of statistical models by analyzing the residual and quantile plots. We consider alternate model formulations and model assumptions in the Supporting Information.

Alternate model form

Although the analyses presented in the main text provide robust tests of the WUE versus CM hypotheses, there are two differences between these two hypotheses. The most fundamental difference is that the pure carbon maximization in the CM hypothesis is the optimal strategy when plants compete for water, whereas the constant marginal water use efficiency in the WUE hypothesis is the optimal strategy when plants do not compete. But the CM hypothesis included carbon costs (as a proxy for risk) of hydraulic damage, whereas the WUE hypothesis model tested thus far does not. Which difference – the optimization criterion or the presence of carbon

costs of hydraulic damage – is responsible for improvements in predictive ability? To answer this question, we also included the risk of hydraulic damage in both models in the Supplementary Methods, so that the only difference between them is the optimization criterion itself. In this broadened form, the WUE hypothesis seeks to maximize $C = A_N - \Theta$ subject to the classic water loss constraint (Cowan & Farquhar 1977; Givnish & others 1986) over a given interval of time. This form gives the broader form of $MXTE_{WUE} = \lambda \frac{dE}{d\psi_L} - \Theta'(\psi_L)$ and allows parsing of whether the improvement in the CM hypothesis is the optimization (constrained versus profit maximization) or the carbon costs of water potential. This analysis further corroborated the initial analysis (in all cases, the CI of λ overlapped zero) and found that both aspects of the CM hypothesis are critical (Fig. S4, S5).

Model assumptions

We next consider some of the assumptions made in our physiological model and how they might influence the results.

Variation in plant hydraulic vulnerability and resistances across tissues could be problematic for using the branch xylem vulnerability curve measured in the vast majority of studies for estimating leaf water potential. We believe this is unlikely to greatly influence our results for several reasons. First, there is a general expectation, which is supported by data (Domec *et al.* 2004; Domec *et al.* 2006; Meinzer *et al.* 2008), that relative hydraulic vulnerabilities of different organs are expected to be coordinated within species. Indeed, a previous modeling study using a similar but more developed hydraulic model on 8 of the same species included here (2 conifers and 6 tropical angiosperms) found that the single branch vulnerability curve was a useful proxy for the whole-plant vulnerability curve and allowed

accurate prediction of measured leaf water potentials (Sperry *et al.* 2016). Third, simulated leaf water potentials generally agreed well with measured leaf water potentials (R^2_{WUE}=0.76, $p<0.0001$; R^2_{CM}=0.8, $p<0.0001$) (Fig. S6). Finally, we expect that as stem water potential values approach the stem embolism threshold, stomata will be closed enough to minimize transpiration-induced differences between stem and leaf water potential.

Cuticular conductance is not directly included in our model, but we do not believe it to be an issue here. The reason is that cuticular conductance is implicitly included in the measurements of stomatal conductance and because we are not trying to estimate a specific stomatal conductance model with a cuticular conductance term, our hydraulics equations implicitly include cuticular conductance within stomatal conductance. Further, a large contribution from cuticular conductance would lead to a biased pattern in the residuals of our predicted versus observed stomatal conductance, which we do not observe (Fig. 2).

Boundary layer conductance is not considered within our physiological model. If boundary layer conductance were small relative to stomatal conductance, this could potentially lead to stomatal response that appeared to be less sensitive to changes in water potential. All else equal, this would primarily decrease the statistical power of the model, expanding the confidence intervals of the parameters and leading to lower explanatory power. The strong fits across all species (Fig. 2) indicate that ignoring boundary layer conductance is likely a reasonable approach, although we acknowledge that uncertainty remains and the lack of boundary layer conductance could be important in several tropical species (e.g. *Ficus insipida* and *Cordia alliodora*) that have relatively poorer model fits, which are species where limiting boundary layer conductances have been observed by previous studies (Andrade *et al.* 1998; Meinzer *et al.* 2004).

Hydraulic capacitance could also potentially give rise to a decoupling between stomata and the transpiration stream at sub-daily timescales, though likely not at longer timescales where soil water potential varies. To examine the potential influence of capacitance, we compared the residuals of predicted versus observed stomatal conductance to the time of day for the seven species with adequate daily data, relying on frequent observations that capacitance discharge occurs primarily in the morning (Meinzer *et al.* 2003, 2004). We observed very few trends in the residuals during the course of a day and thus do not believe this is a large concern for our analysis.

Non-stomatal limitation of photosynthesis can occur and is likely important under severe drought conditions (Flexas & Medrano 2002). In theory, this cost to the plant is included in our CM hypothesis because we do not specify where the costs come from and the direct effects of low water potentials on the photosynthetic machinery would be included in these costs. The reasonable prediction of photosynthesis compared to measured photosynthesis values (Fig. S7) supports our model because photosynthesis was not fit at any stage (only stomatal conductance is fit via the parameter estimation procedure). Direct effects of drought on photosynthesis have been shown to lead to variable V_{cmax} in some species, including two species analyzed here (Xu & Baldocchi 2003; Martin-StPaul *et al.* 2013). We tested for the potential importance of variable V_{cmax} on a random subset of 8 species, including the two oak species where V_{cmax} has been documented to change over the course of a season. For this analysis, after fitting K_{max} we further fit V_{cmax} for every datapoint or for every day using the observed photosynthesis and stomatal conductance measurements before running the parameter estimation. We compared the variable V_{cmax} and fixed V_{cmax} models with Akaike Information Criterion that accounts for the increased number of parameters. We found that variable V_{cmax} improved prediction (i.e. $\Delta AIC < -3$) only in

116 the two oak species that it had been observed in previously (*Quercus ilex* and *Quercus douglasii*)
117 and *Prosopis velutina* and thus used variable V_{cmax} in those species for all subsequent analyses
118 and fixed V_{cmax} in all other species.
119
120 *Scaling up stomatal conductance optimizations in a land surface model*
121 We used the Geophysical Fluid Dynamics Laboratory's Land-Model 3 with Perfect
122 Plasticity Approximation (GFDL LM3-PPA) land surface model (Weng *et al.* 2015) to perform
123 first-order tests of the potential magnitude of implementing a hydraulic stomatal control
124 algorithm consistent with the CMH optimization. LM3-PPA is a full land surface model built to
125 be coupled to the GFDL Earth system model and calculates fluxes of carbon, water, and energy
126 at half-hour time-steps. Critically, this model uses the "perfect plasticity approximation" (PPA)
127 algorithm, which assumes that plants can bend to grow towards the light and fill a canopy, to
128 simulate cohorts of vegetation (trees) that compete for water, nutrients, and light. This enables
129 the implementation of a tree hydraulic schema that can calculate water transport from the soil to
130 canopy (including tree height effects) and leaf water potential, which can be used to influence
131 stomatal conductance. The previous implementation of stomatal control used one of the standard
132 empirical models (Leuning 1995), which is consistent with the WUE optimization approach over
133 most conditions (Medlyn *et al.* 2011), accounting for soil moisture constraints using a "supply-
134 demand" approach where soil moisture constrained supply.
135 Water limitation in LSMs generally take one of two forms, both of which use soil
136 moisture as an endogenous state variable to impose a limitation on evapotranspiration, and have
137 no mechanistic connection to physiology in the canopy, where the valves that reduce ET are
138 located (as in this paper). The first method is known as the "Jarvis-type" soil moisture limitation,

and multiplies the default ET (calculated, e.g. by Ball-Leuning-Berry) by a scalar ranging from 0 to 1 which depends on soil moisture. The exact shape of this function varies depending on the model and species/plant-functional-type under consideration. The second method, used in GFDL's LM3 is less widely adopted because it has more sophisticated computational requirements. In this method, the flux of soil moisture from the soil to the root is estimated using the integral of the unsaturated soil moisture characteristic curve imposed by the driving gradient of water potential from the root surface to the bulk soil. This scheme preserves mass (i.e. water) and energy (i.e. potential), but most relevant here it imposes a limit to the amount of water supplied to the plant as a function of soil properties and soil water potential. ET in LSM is then set as the minimum of the unstressed ET (demand driven) and soil moisture flux (supply driven). The new hydraulic framework described below is a unification of the supply and demand, in essence finding a solution water potential where supply and demand are equal, which is conceptually similar to solving the combined photosynthesis and Ball-Berry-Leuning model for the equilibrium leaf CO_2 that satisfies supply and demand, or solving the Penman-Monteith by solving the equilibrium leaf surface temperature.

The model was implemented at the Missouri Ozark Ameriflux site in Missouri, USA, because it contained concurrent eddy flux data and measurements of leaf water potentials. The default model parameters described in (Weng *et al.* 2015) were used except the tree species was parameterized for one of the dominant species – *Quercus alba*. The following parameter values were changed to capture the key components of *Quercus alba* physiology: Xylem c parameter = -2.0, xylem d parameter = 1.5; water potential at leaf turgor loss: -4.5 MPa ; LMA = 0.86e-01; Vcmax = 0.45e-04; rho_wood = 317.0 (units as in (Weng *et al.* 2015)), values drawn from (Kattge *et al.* 2011; Bartlett *et al.* 2014; Gleason *et al.* 2015). The forest was spun up from 1700-

1980 using the looped 1948-1979 climatology period from the Sheffield dataset (Sheffield *et al.* 2006). Leaf area index and NPP reasonably reflected observed values at the site. The model spin-up period used the default water stress scheme. Subsequently, a simulation using the default scheme and a simulation using the new hydraulic-stomata scheme (below) were each run from 1980-2008 using the Sheffield data for that time period. Because both simulations used the same spin up (thus starting with identical carbon and water pools and forest demography) and the same forcing data, all differences between the models should reflect the stomatal algorithm. We focus on the years 2006-2008, where two very dry years were documented in 2006-2007, followed by a wet year in 2008 (Gu *et al.* 2015). For these years, we summed the latent energy exchange for the growing season (DOY 100-300) for both water stress formulations. The larger decline in latent energy in 2007 is consistent with two years of drought in a row leading to lower soil water potentials during the second year, but full examination and comparison of these algorithms to flux data will require separate treatment.

New hydraulic-stomata scheme in the land surface model

While the full behavior of the new water stress scheme in LM3-PPA will require separate treatment, we describe here the core components that allowed a first order test of ecosystem water fluxes in the two different stomatal algorithms. In the new water stress scheme, stomatal conductance and photosynthesis are first calculated using the standard iterative procedure described in (Collatz *et al.* 1991). This is considered a "potential stomatal conductance" absent water stress constraints. The water required to meet that stomatal conductance is calculated. Next, water flux from the soil to the roots and from the roots up to the sub-stomatal pore is calculated as a series of resistances (soil-root, root xylem, stem xylem, and leaf xylem)

formulated in Richard's equations, per (Sperry *et al.* 1998). The flux of water is solved using integral transforms (approximated as an incomplete gamma function) across these water potential gradients. In theory, each of these elements can have a different vulnerability curve, but data is rarely available to parameterize these curves. Thus, as is commonly done (Mackay *et al.* 2015; Sperry *et al.* 2016), we assume that the stem vulnerability curve can be used to approximate the whole-plant curve. Next, stomatal sensitivity to water potential is captured by an additional stomatal conductance equation as a Weibull function of leaf water potential. While the LSM is not implementing the CM optimization directly, this stomatal sensitivity to leaf water potential is the identical functional form of the CM hypothesis derived in Wolf et al. 2016 for simplified conditions (e.g. an exact analog of the approach of how the WUE hypothesis has been incorporated into LSMs recently (De Kauwe *et al.* 2015; Kala *et al.* 2015)). The parameter c of the Weibull function is determined by the measured species' leaf turgor loss point, such that the 95% loss of stomatal conductance occurs around leaf turgor loss (Bartlett *et al.* 2016). Finally, transpiration and stomatal conductance are determined such that water demand is capped by water supply provided via the hydraulic continuum to the leaf. The strengths of this model are that it 1) incorporates in soil water potential, 2) translates soil water potential through species-specific xylem and stomatal traits to leaf water potential, 3) can be parameterized by traits commonly measured in the ecophysiology literature 4) provides a direct feedback mechanism of leaf water potential on stomatal conductance, and 5) yields a stomatal optimization consistent with the CM hypothesis (Wolf *et al.* 2016).

Supplementary Tables and Table Legends

Table S1: Species included in the analysis with their biome (needleleaf evergreen temperate (NET), broadleaf evergreen temperate (BET), broadleaf deciduous temperate (BDT), tropical deciduous (TPD), and tropical evergreen (TPE), references of studies (Xu & Baldocchi 2003; Meinzer *et al.* 2004; Choat *et al.* 2006; Resco *et al.* 2009; Arango-Velez *et al.* 2011; Anderegg 2012; Koepke & Kolb 2013; Limousin *et al.* 2013; Martin-StPaul *et al.* 2013; Lin *et al.* 2015; Chmura *et al.* 2016; Hernandez *et al.* 2016; Li *et al.* 2015; Wolfe *et al.* 2016), the "c" and "d" parameters of the Weibull hydraulic vulnerability curve from Gleason *et al.* (2015) sample size of stomatal conductance measurements (N), and V_{cmax} at 25 C (with V indicating varying V_{cmax}).

Species name	Biome	Wbc	Wbd	N	V_{cmax}	Reference
Acer campestre	BDT	4.8	3.8	41	36.6	Li et al. 2015
Acer pseudoplatanus	BDT	3.3	3.2	39	50	Li et al. 2015
Alphitonia excelsa	TPE	6.2	2	173	42.9	Choat et al. 2006
Anacardium excelsum	TPD	1.8	2.1	14	27.2	Meinzer et al. 2004
Annona hayesii	TPD	5	4.3	46	13.6	Wolfe et al. 2016
Astronium graveolens	TPE	4.9	3.3	91	19.7	Wolfe et al. 2016
Austromyrtus bidwillii	TPE	6.4	1.4	35	28.5	Choat et al. 2006
Brachychiton australis	TPD	3.6	1.9	100	57.2	Choat et al. 2006
Bursera simaruba	TPD	1.4	3.2	104	17.4	Wolfe et al. 2016
Carpinus betulus	BDT	4	3.8	48	31.4	Li et al. 2015
Cavanillesia platanifolia	TPD	1.3	2.3	41	11.6	Wolfe et al. 2016
Cochlospermum gillivraei	TPD	2	1.4	75	52.1	Choat et al. 2006
Cojoba rufescens	TPE	4.5	2	319	26.4	Wolfe et al. 2016
Cordia alliodora	TPD	3.3	1.7	18	69	Meinzer et al. 2004
Corylus avellana	BDT	2.3	3.5	35	20.4	Li et al. 2015
Eucalyptus globulus	BET	1.6	1.4	73	81.7	Hernandez et al. 2016
Ficus insipida	TPE	2.3	1.4	14	74.6	Meinzer et al. 2004
Fraxinus excelsior	BDT	3	2.9	40	65	Li et al. 2015
Genipa americana	TPD	2.7	1.3	109	26	Wolfe et al. 2016
Juniperus monosperma	NET	8.8	3	576	40	Limousin et al. 2013

Juniperus osteosperma	NET	9	3	34	31.3	Koepke & Kolb 2013
Phillyrea angustifolia	BET	9.9	6	17	12.9	Resco et al. 2009
Picea abies	NET	4.7	3.3	544	43	Chmura et al. 2015
Pinus edulis	NET	4	6	511	35	Limousin et al. 2013
Pinus ponderosa	NET	3.75	3.2	146	35	Kolb & Stone 1999
Pistacia lentiscus	BET	3.5	1.6	23	37	Resco et al. 2009
Populus balsamifora	BDT	2	2.5	29	50.9	Arango-Velez et al. 2011
Populus tremuloides	BDT	2.7	2	43	95	Anderegg 2012
Prosopis velutina	BDT	2.98	1.19	23	V	Lin et al. 2015
Quercus douglasii	BET	2.1	0.3	166	V	Xu & Baldochhi 2003
Quercus gambelii	BDT	0.6	1	12	84.6	Kolb & Stone 1999
Quercus ilex	BET	4.2	1.4	110	V	St. Paul et al. 2012
Schefflera morototoni	TPE	1.85	3.4	19	69.1	Meinzer et al. 2004
Tapirira guianensis	TPE	2	1.6	33	21.6	Meinzer et al. 2004

Table S2: Environmental conditions experienced by species included in the analysis: the sample size of stomatal conductance measurements (N), "c" parameters of the Weibull hydraulic vulnerability curve, minimum leaf water potential experienced by the species (ψ_{Lmin}, MPa), maximum leaf water potential experienced by the species (ψ_{Lmax}, MPa), and minimum stomatal conductance measured for the species (g_{smin}, mol m^{-2} sec^{-1}). *ψ_{Lmax} estimated from hydraulics equations. ^ψ_{Lmin} estimated from hydraulics equations.

Species name	**N**	**Weib c**	ψ_{Lmin}	ψ_{Lmax}	g_{smin}
Acer campestre	41	4.8	-5.57	-0.24*	0.0000
Acer pseudoplatanus	39	3.3	-6.6	-0.05*	0.0027
Alphitonia excelsa	173	6.2	-5.45	-0.20	0.0000
Anacardium excelsum	14	1.8	-0.75	-0.30	0.0510
Annona hayesii	46	5	-3.36	-0.35	0.0074
Astronium graveolens	91	4.9	-3.41	-0.44	0.0066
Austromyrtus bidwillii	35	6.4	-2.5	-0.20	0.0100
Brachychiton australis	100	3.6	-2.5	-0.18	0.0000
Bursera simaruba	101	1.4	-1.03	-0.43	0.0010
Carpinus betulus	48	4	-4.85	-0.49*	0.0138
Cavanillesia platanifolia	41	1.3	-0.86	-0.35	0.0049
Cochlospermum gillivraei	75	2	-1.75	-0.28	0.0100
Cojoba rufescens	319	4.5	-4.4	-0.42	0.0007
Cordia alliodora	18	3.3	-2.5625	-0.75	0.1307
Corylus avellana	35	2.3	-3.44	-0.78*	0.0066
Eucalyptus globulus	73	1.6	-1.75	-0.80*	0.0340
Ficus insipida	14	2.3	-1.25	-0.40	0.0985
Fraxinus excelsior	40	3	-4.35	-0.05*	0.0130
Genipa americana	109	2.7	-2.73	-0.48	0.0042
Juniperus monosperma	576	8.8	-7	-0.67	0.0018
Juniperus osteosperma	34	9	-3.6	-1.07	0.0403
Phillyrea angustifolia	17	9.9	-2.38	-2.28	0.0600
Picea abies	544	4.7	-3.52	-0.07	0.0058
Pinus edulis	511	4	-3.7	-0.68	0.0020
Pinus ponderosa	146	3.75	-2.02	-0.47	0.0209
Pistacia lentiscus	23	3.5	-1.5^	-1.05	0.0360
Populus balsamifora	29	2	-1.05	-0.05*	0.1440

Populus tremuloides	43	2.7	-2	-0.15	0.0052
Prosopis velutina	23	2.98	-7^	-0.12	0.0433
Quercus douglasii	166	2.1	-3.52	-0.30	0.0082
Quercus gambelii	12	0.6	-2.53	-0.16	0.0449
Quercus ilex	110	4.2	-4^	-0.35	0.0065
Schefflera morototoni	19	1.85	-1.775	-0.30	0.1050
Tapirira guianensis	33	2	-1.45	-0.44	0.0909

257 Table S3: Mathematical symbols used throughout the manuscript, their definition, units, and

258 their use in the model as input, output, fixed parameter, or estimated parameter.

Symbol	Definition	Units	Status
g_s	Stomatal conductance	mol m^{-2} s^{-1}	Model output
C	Carbon gain as the balance of net assimilation minus the carbon costs incurred by a given water potential	μmol m^{-2} s^{-1}	NA
A_n	Net assimilation (photosynthesis minus respiration) of the leaf	μmol m^{-2} s^{-1}	Model output
Θ	Carbon costs of the risk of a given water potential	μmol m^{-2} s^{-1}	NA
Θ′	Marginal carbon costs of the risk of a given water potential (partial derivative of Θ with respect to leaf water potential)	μmol m^{-2} s^{-1} MPa^{-1}	CM: Estimated parameter
ψ_L	Leaf water potential	MPa	Model output
ψ_S	Soil water potential	MPa	Input variable
ψ	Tissue water potential	MPa	NA
K	Hydraulic conductance to water	mmol m^{-2} s^{-1} MPa^{-1}	Model output
E	Transpiration	mmol m^{-2} s^{-1}	Model output
λ	Marginal water use efficiency (here $\partial A_N/\partial E$) in the WUE optimization	μmol /mmol	WUE: Estimated parameter
C_i	Internal leaf CO_2 concentration	ppm	Model output
C_a	Atmospheric CO_2 concentration at the leaf surface	ppm	Input variable
PAR	Photosynthetically active radiation	μmol m^{-2} s^{-1}	Input variable
a	Slope of the Θ′ function	μmol m^{-2} s^{-1} MPa^{-2}	CM: Estimated parameter
b	Intercept of the Θ′ function	μmol m^{-2} s^{-1} MPa^{-1}	CM: Estimated parameter
β_1	Slope of the marginal xylem tension efficiency function	μmol m^{-2} s^{-1} MPa^{-2}	Estimated parameter
B_0	Intercept of the marginal xylem tension efficiency function	μmol m^{-2} s^{-1} MPa^{-1}	Estimated parameter
V_{cmax}	Maximum rate of carboxylation at 25 C	μmol m^{-2} s^{-1}	Fixed parameter
K_{max}	Maximum hydraulic conductance through the hydraulic continuum	mmol m^{-2} s^{-1} MPa^{-1}	Fixed parameter

259 Table S4: Sensitivity analyses of the slope of the MXTE to 10% change in input of species'
260 xylem and photosynthetic traits – the maximum hydraulic conductance (K) and the maximum
261 carboxylation rate at 25 C (V).

Species	Original	K-10%	K+10%	V-10%	V+10%
Quercus gambelii	-10.13	-5.83	-12.57	-9.39	-9.02
Pistacia lentiscus	-6.39	-4.92	-7.96	-0.74	-7.42
Populus tremuloides	-9.79	-16.29	-6.41	-17.01	-5.28
Austromyrtus bidwillii	1.54	1.33	1.84	1.31	1.89
Pinus ponderosa	-12.48	-11.11	-13.83	-11.02	-13.26

262
263
264
265
266
267
268
269
270
271
272
273
274
275
276
277
278

Supplementary Figures

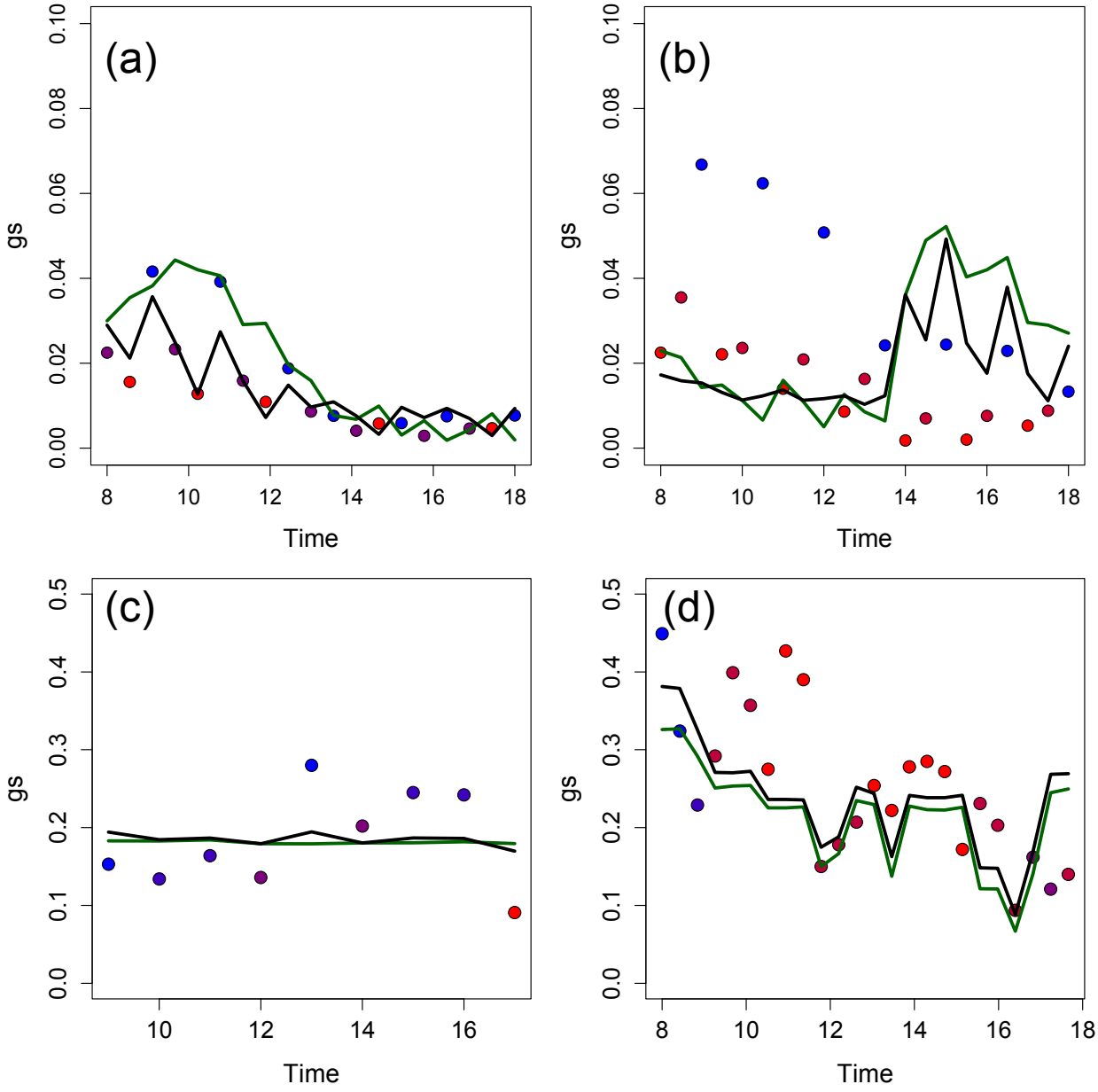

Figure S1: Illustrative time-series (time of day) of observed (dots) and predicted stomatal conductance for the CMH (black line) and WUEH (green line) over individual days for *Pinus edulis* (a,b) and *Tapirira guianensis* (c,d). Colors in (a,b) represent soil water potential of different individual trees measured and in (c,d) represent leaf water potential with red indicating more negative water potentials.

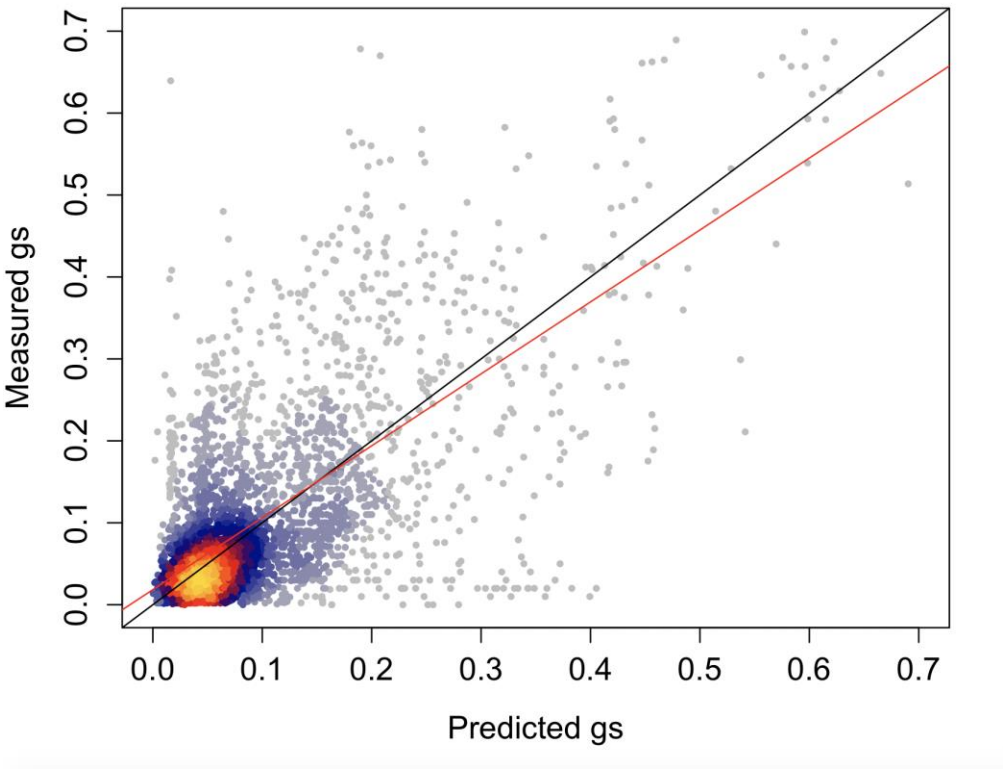

286

287 Figure S2: The predicted versus measured stomatal conductance (gs; mol m^{-2} sec^{-1}) for models fit
288 on each of 34 species for the WUE with λ modified by a non-linear function of soil water
289 potential (R^2=0.52). Black lines represent the 1:1 line and red lines are the best fit for
290 ordinary least squares regression. Colors indicate the density of points from highest
291 density (yellow) to lowest (blue to gray).

292

293

294

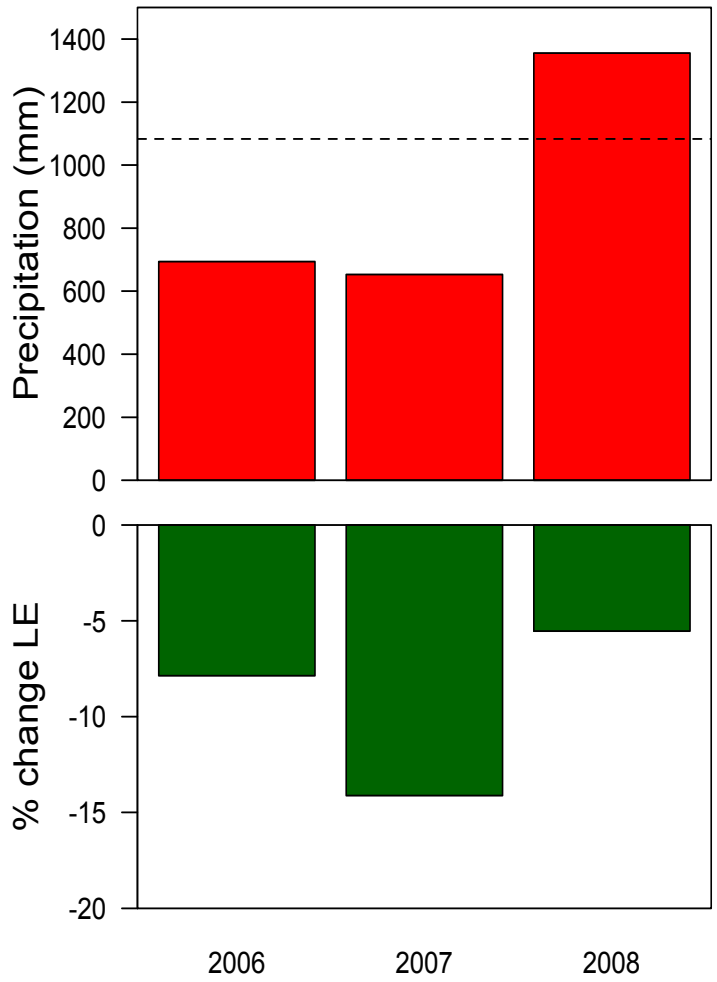

Figure S3: Precipitation at the Missouri Ozark Ameriflux site from 2006-2008 (dashed line is the 1970-2000 average) (top). Change in latent energy exchange (%) between the default water stress scheme in the LM3-PPA land surface model and the hydraulic-stomatal water stress scheme (bottom).

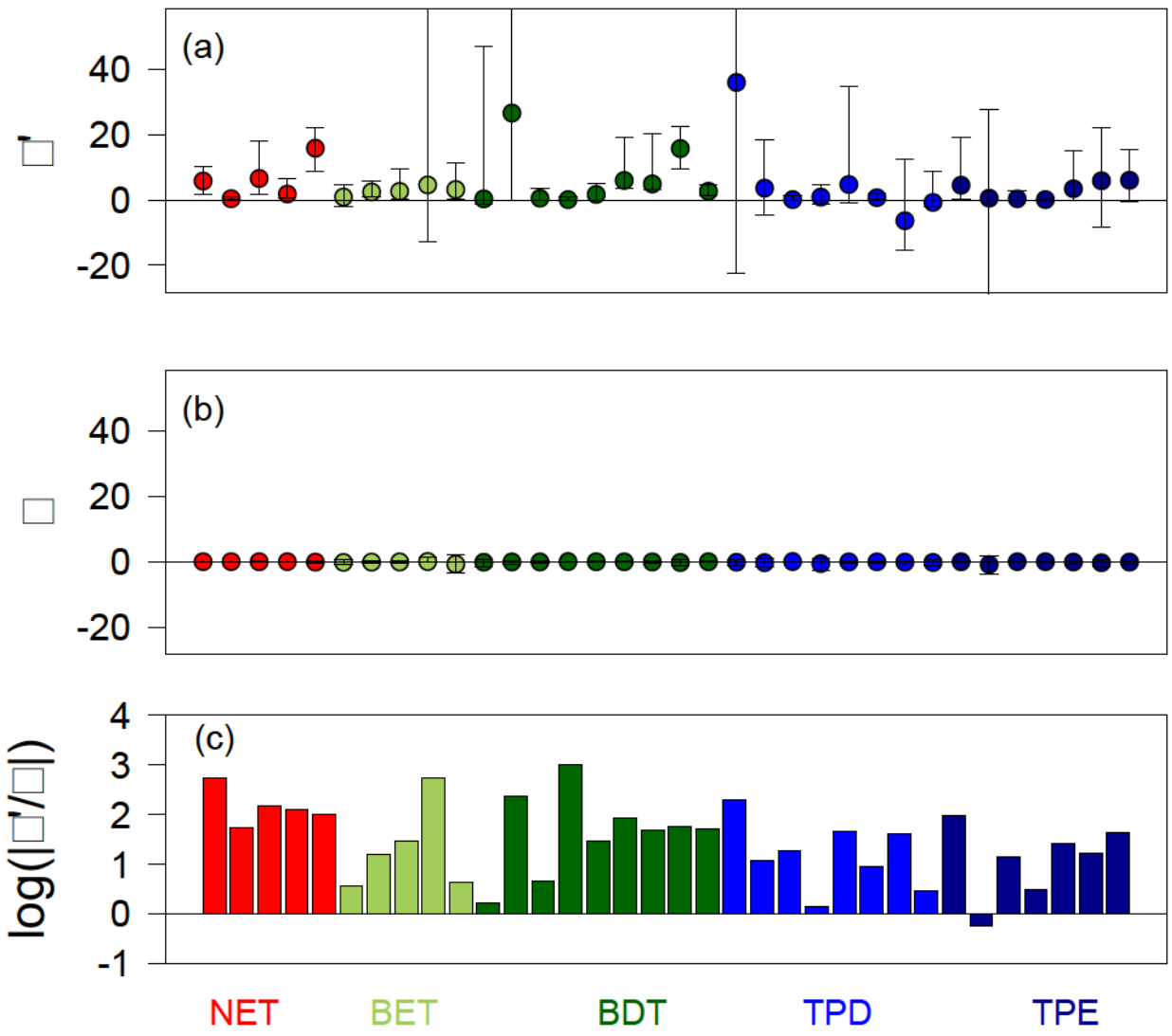

Fig. S4: MXTE functions support the carbon maximization optimization. (a) The opposite of the slope of the MXTE function ($-\Theta'(\psi_L)$) shown across biomes (NET: needleleaf evergreen temperate; BET: broadleaf evergreen temperate; BDT: broadleaf deciduous temperate; TPD: tropical deciduous; TPE: tropical evergreen). Error bars are the 95% confidence intervals. (b) The estimated dA/dE (λ) values of the marginal cost function. (c) The $\log_{10}$ of the absolute value of the slope of the marginal cost function divided by the dA/dE (λ), where positive values indicate $\Theta' > \lambda$ and values of >1 indicate $\Theta' >> \lambda$.

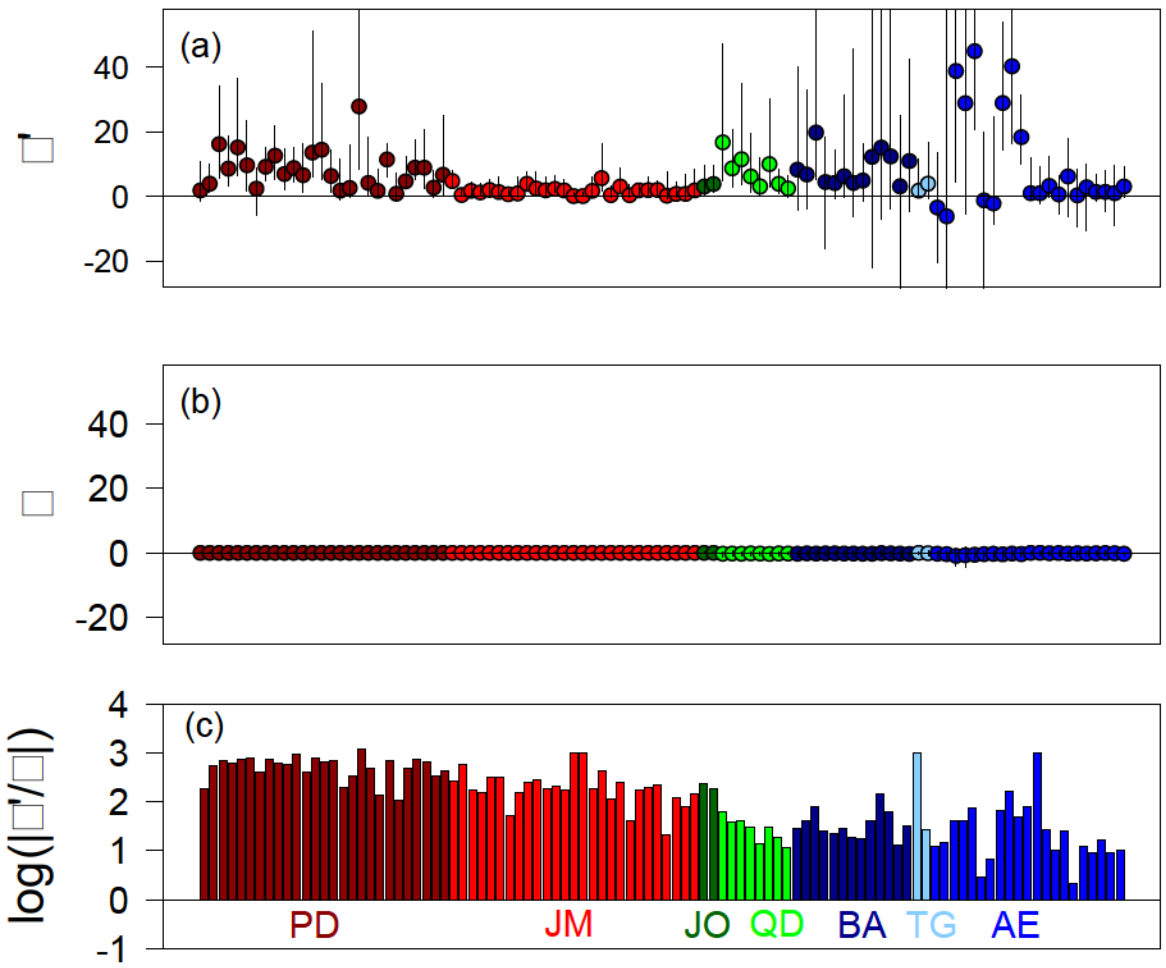

309

310 Figure S5: MXTE functions support the carbon maximization optimization at daily timescales.
311 (a) The opposite of the slope ($-\beta_1$) of the MXTE function ($\Theta'(\psi_L)$) shown across 7 species with
312 adequate data (PD: *Pinus edulis*; JM: *Juniperus monosperma*; JO: *Juniperus osteosperma*; QD:
313 *Quercus douglasii*; BA: *Brachychiton australis*; TG: *Tapirira guianensis*; AE: *Alphitonia*
314 *excelsa*). Error bars are the 95% confidence intervals. (b) The estimated dA/dE (λ) values of the
315 marginal cost function. (c) The $\log_{10}$ of the absolute value of the slope of the marginal cost
316 function divided by the dA/dE (λ), where positive values indicate $\Theta' > \lambda$ and values of >1
317 indicate $\Theta' >> \lambda$.

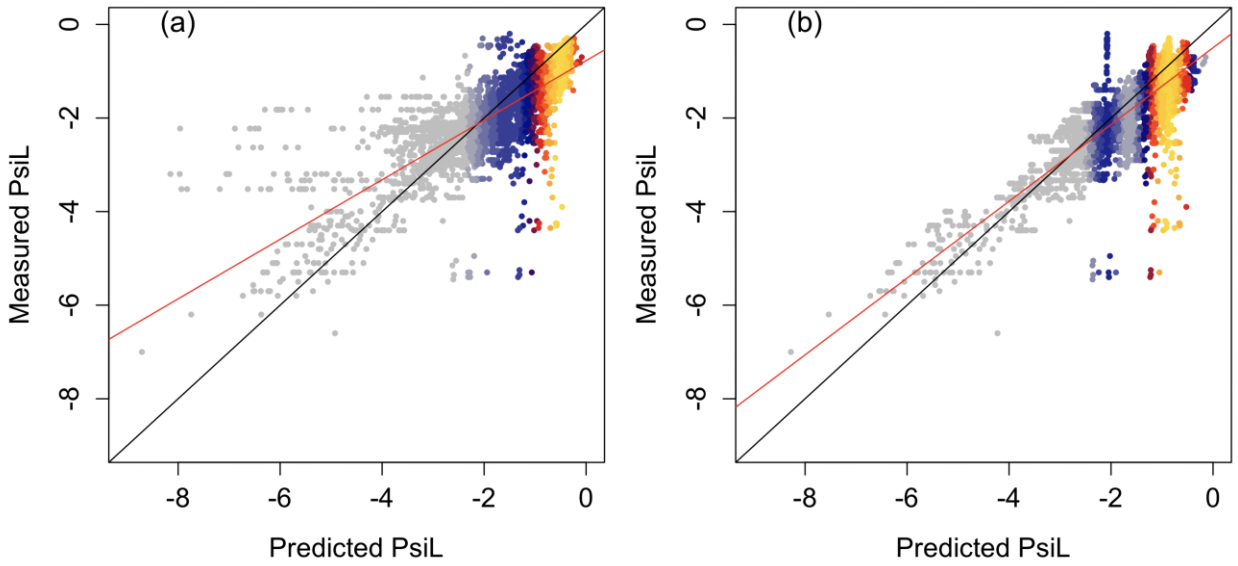

Figure S6: Heat scatterplot of estimates of the predicted leaf water potential (MPa) versus the observed leaf water potential estimates of all species combined for the WUEH (a) and CMH (b) (R^2_{WUEH}=0.76, p<0.0001; R^2_{CMH}=0.8, p<0.0001). Colors signify the density of points in a given region from low (gray) to high (yellow) density. Black line is the 1:1 line and red line is the OLS regression best fit.

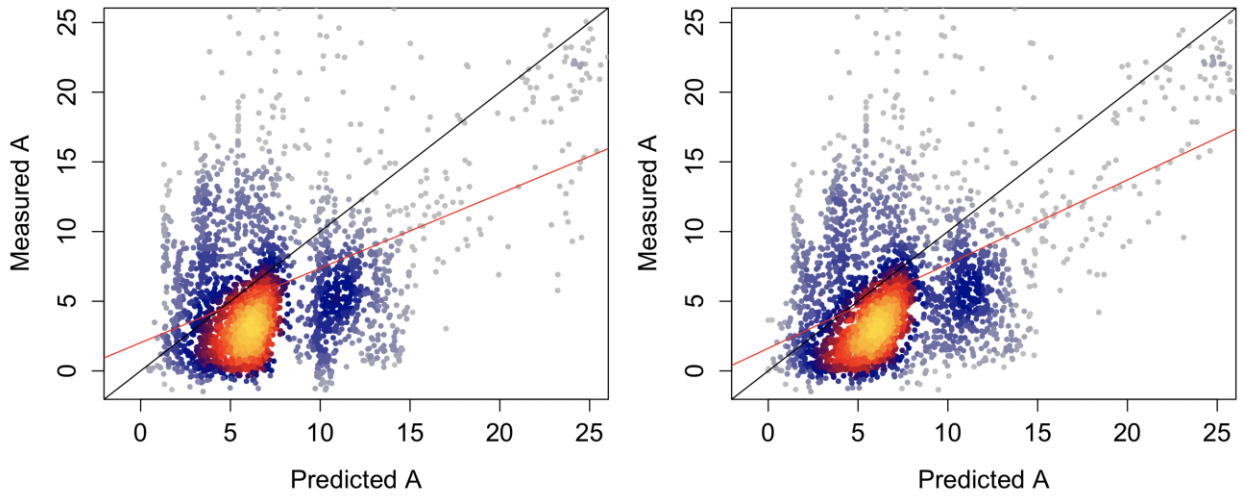

Figure S7: Heat scatterplot of estimates of the predicted photosynthesis (A; µmol*m^{-2}*s^{-1}) versus the observed photosynthesis estimates of all species combined for the WUEH (a) and CMH (b). Colors signify the density of points in a given region from low (gray) to high (yellow) density. Black line is the 1:1 line and red line is the OLS regression best fit.

References

Anderegg, W. (2012). Complex aspen forest carbon and root dynamics during drought. *Clim. Change*, 111, 983–991.

Andrade, J.L., Meinzer, F.C., Goldstein, G., Holbrook, N.M., Cavelier, J., Jackson, P., *et al.* (1998). Regulation of water flux through trunks, branches, and leaves in trees of a lowland tropical forest. *Oecologia*, 115, 463–471.

Arango-Velez, A., Zwiazek, J.J., Thomas, B.R. & Tyree, M.T. (2011). Stomatal factors and vulnerability of stem xylem to cavitation in poplars. *Physiol. Plant.*, 143, 154–165.

Bartlett, M.K., Klein, T., Jansen, S., Choat, B. & Sack, L. (2016). The correlations and sequence of plant stomatal, hydraulic, and wilting responses to drought. *Proc. Natl. Acad. Sci.*, 113, 13098–13103.

Bartlett, M.K., Zhang, Y., Kreidler, N., Sun, S., Ardy, R., Cao, K., *et al.* (2014). Global analysis of plasticity in turgor loss point, a key drought tolerance trait. *Ecol. Lett.*, 17, 1580–1590.

Chmura, D.J., Guzicka, M., McCulloh, K.A. & Żytkowiak, R. (2016). Limited variation found among Norway spruce half-sib families in physiological response to drought and resistance to embolism. *Tree Physiol.*, 36, 252–266.

Choat, B., Ball, M.C., Luly, J.G., Donnelly, C.F. & Holtum, J.A. (2006). Seasonal patterns of leaf gas exchange and water relations in dry rain forest trees of contrasting leaf phenology. *Tree Physiol.*, 26, 657–664.

Collatz, G.J., Ball, J.T., Grivet, C. & Berry, J.A. (1991). Physiological and environmental regulation of stomatal conductance, photosynthesis and transpiration: a model that includes a laminar boundary layer. *Agric. For. Meteorol.*, 54, 107–136.

Cowan, I.R. & Farquhar, G.D. (1977). Stomatal function in relation to leaf metabolism and environment. In: *Symposia of the Society for Experimental Biology*. p. 471.

De Kauwe, M.G., Kala, J., Lin, Y.S., Pitman, A.J., Medlyn, B.E., Duursma, R.A., *et al.* (2015). *A test of an optimal stomatal conductance scheme within the CABLE land surface model, Geosci. Model Dev., 8, 431–452*.

Domec, J.-C., Scholz, F.G., Bucci, S.J., Meinzer, F.C., Goldstein, G. & Villalobos-Vega, R. (2006). Diurnal and seasonal variation in root xylem embolism in neotropical savanna woody species: impact on stomatal control of plant water status. *Plant Cell Environ.*, 29, 26–35.

Domec, J.-C., Warren, J.M., Meinzer, F.C., Brooks, J.R. & Coulombe, R. (2004). Native root xylem embolism and stomatal closure in stands of Douglas-fir and ponderosa pine: mitigation by hydraulic redistribution. *Oecologia*, 141, 7–16.

Flexas, J. & Medrano, H. (2002). Drought-inhibition of photosynthesis in C3 plants: stomatal and non-stomatal limitations revisited. *Ann. Bot.*, 89, 183–189.

Givnish, T.J. & others. (1986). Optimal stomatal conductance, allocation of energy between leaves and roots, and the marginal cost of transpiration. In: *On the economy of plant form and function*. Cambridge University Press, pp. 171–213.

Gleason, S.M., Westoby, M., Jansen, S., Choat, B., Hacke, U.G., Pratt, R.B., *et al.* (2015). Weak tradeoff between xylem safety and xylem-specific hydraulic efficiency across the world's woody plant species. *New Phytol.*, 209, 123–136.

386 Gu, L., Pallardy, S.G., Hosman, K.P. & Sun, Y. (2015). Drought-influenced mortality of tree
387 species with different predawn leaf water dynamics in a decade-long study of a central
388 US forest. *Biogeosciences*, 12, 2831–2845.
389 Hernandez, M.J., Montes, F., Ruiz, F., Lopez, G. & Pita, P. (2016). The effect of vapour pressure
390 deficit on stomatal conductance, sap pH and leaf-specific hydraulic conductance in
391 Eucalyptus globulus clones grown under two watering regimes. *Ann. Bot.*, 117, 1063–
392 1071.
393 Kala, J., De Kauwe, M.G., Pitman, A.J., Lorenz, R., Medlyn, B.E., Wang, Y.-P., *et al.* (2015).
394 Implementation of an optimal stomatal conductance model in the Australian Community
395 Climate Earth Systems Simulator (ACCESS1. 3b). *Geosci. Model Dev. Discuss.*, 8.
396 Kattge, J., DÍAz, S., Lavorel, S., Prentice, I.C., Leadley, P., BÖNisch, G., *et al.* (2011). TRY – a
397 global database of plant traits. *Glob. Change Biol.*, 17, 2905–2935.
398 Koepke, D.F. & Kolb, T.E. (2013). Species variation in water relations and xylem vulnerability
399 to cavitation at a forest-woodland ecotone. *For. Sci.*, 59, 524–535.
400 Leuning, R. (1995). A critical appraisal of a combined stomatal-photosynthesis model for C3
401 plants. *Plant Cell Environ.*, 18, 339–355.
402 Li, S., Feifel, M., Karimi, Z., Schuldt, B., Choat, B. & Jansen, S. (2015). Leaf gas exchange
403 performance and the lethal water potential of five European species during drought. *Tree*
404 *Physiol.*, 36, 179–192.
405 Limousin, J., Bickford, C.P., Dickman, L.T., Pangle, R.E., Hudson, P.J., Boutz, A.L., *et al.*
406 (2013). Regulation and acclimation of leaf gas exchange in a piñon–juniper woodland
407 exposed to three different precipitation regimes. *Plant Cell Environ.*, 36, 1812–1825.
408 Lin, Y.-S., Medlyn, B.E., Duursma, R.A., Prentice, I.C., Wang, H., Baig, S., *et al.* (2015).
409 Optimal stomatal behaviour around the world. *Nat. Clim. Change*, 5, 459–464.
410 Mackay, D.S., Roberts, D.E., Ewers, B.E., Sperry, J.S., McDowell, N.G. & Pockman, W.T.
411 (2015). Interdependence of chronic hydraulic dysfunction and canopy processes can
412 improve integrated models of tree response to drought. *Water Resour. Res.*
413 Martin-StPaul, N.K., Limousin, J.-M., Vogt-Schilb, H., Rodríguez-Calcerrada, J., Rambal, S.,
414 Longepierre, D., *et al.* (2013). The temporal response to drought in a Mediterranean
415 evergreen tree: comparing a regional precipitation gradient and a throughfall exclusion
416 experiment. *Glob. Change Biol.*, 19, 2413–2426.
417 Medlyn, B.E., Duursma, R.A., Eamus, D., Ellsworth, D.S., Prentice, I.C., Barton, C.V.M., *et al.*
418 (2011). Reconciling the optimal and empirical approaches to modelling stomatal
419 conductance. *Glob. Change Biol.*, 17, 2134–2144.
420 Meinzer, F.C., James, S.A. & Goldstein, G. (2004). Dynamics of transpiration, sap flow and use
421 of stored water in tropical forest canopy trees. *Tree Physiol.*, 24, 901–909.
422 Meinzer, F.C., James, S.A., Goldstein, G. & Woodruff, D. (2003). Whole-tree water transport
423 scales with sapwood capacitance in tropical forest canopy trees. *Plant Cell Environ.*, 26,
424 1147–1155.
425 Meinzer, F.C., Woodruff, D.R., Domec, J.-C., Goldstein, G., Campanello, P.I., Gatti, M.G., *et al.*
426 (2008). Coordination of leaf and stem water transport properties in tropical forest trees.
427 *Oecologia*, 156, 31–41.
428 Resco, V., Ewers, B.E., Sun, W., Huxman, T.E., Weltzin, J.F. & Williams, D.G. (2009).
429 Drought-induced hydraulic limitations constrain leaf gas exchange recovery after

precipitation pulses in the C3 woody legume, Prosopis velutina. *New Phytol.*, 181, 672–682.

Sheffield, J., Goteti, G. & Wood, E.F. (2006). Development of a 50-Year High-Resolution Global Dataset of Meteorological Forcings for Land Surface Modeling. *J. Clim.*, 19, 3088–3111.

Sperry, J.S., Adler, F.R., Campbell, G.S. & Comstock, J.P. (1998). Limitation of plant water use by rhizosphere and xylem conductance: results from a model. *Plant Cell Environ.*, 21, 347–359.

Sperry, J.S., Wang, Y., Wolfe, B.T., Mackay, D.S., Anderegg, W.R., McDowell, N.G., *et al.* (2016). Pragmatic hydraulic theory predicts stomatal responses to climatic water deficits. *New Phytol ., 212, 577-589.*

Weng, E.S., Malyshev, S., Lichstein, J.W., Farrior, C.E., Dybzinski, R., Zhang, T., *et al.* (2015). Scaling from individual trees to forests in an Earth system modeling framework using a mathematically tractable model of height-structured competition. *Biogeosciences*, 12, 2655–2694.

Wolf, A., Anderegg, W.R. & Pacala, S.W. (2016). Optimal stomatal behavior with competition for water and risk of hydraulic impairment. *Proc. Natl. Acad. Sci.*, 113, E7222–E7230.

Wolfe, B.T., Sperry, J.S. & Kursar, T.A. (2016). Does leaf shedding protect stems from cavitation during seasonal droughts? A test of the hydraulic fuse hypothesis. *New Phytol.*, 212, 1007–1018.

Xu, L. & Baldocchi, D.D. (2003). Seasonal trends in photosynthetic parameters and stomatal conductance of blue oak (Quercus douglasii) under prolonged summer drought and high temperature. *Tree Physiol.*, 23, 865–877.